Electronic Supplementary Information

Potential anion sensing properties by a redox and substitution series of $[Ru(bpy)_{3-n}(Hdpa)_n]^{2+}$, n = 1−3; Hdpa = 2,2′-Dipyridylamine: selective recognition and stoichiometric binding with cyanide and fluoride ions

Sagar K. Patil,[a] Rajib Ghosh,[b] Princy Kennedy,[a] Shaikh M. Mobin[c] and Dipanwita Das*[a]

[a]Department of Chemistry, Institute of Chemical Technology, Matunga, Mumbai 400019 (India)

Fax: (91)022-3361-1020

E-mail: dr.das@ictmumbai.edu.in

[b]Radiation and Photochemistry Division, Bhabha Atomic Research Centre, Mumbai-400094, India

[c]Discipline of Chemistry, School of Basic Sciences, Indian Institute of Technology Indore, Indore 452017, India

Table S1 Crystallographic data for $[Ru(bpy)(Hdpa)_2](ClO_4)_2$ [**2**]$(ClO_4)_2$ and $[Ru(bpy)_2(dpa)](BF_4)$ [**1**](BF_4)

	[**2**]$(ClO_4)_2$	[**1**]BF_4
Formula	$C_{30}H_{26}Cl_2N_8O_8Ru$	$C_{30}H_{24}BF_4N_7Ru$
Fw	798.56	670.44
T(K)	293(2) K	293 (2) K
Cryst. Syst.	Triclinic	Trigonal
Space group	*P*-1	*P*3221
a /Å	8.1459(5)	13.0588(3)
b /Å	10.9387(5)	13.0588(3)
c /Å	17.8507(9)	31.5888(11)
α (º)	88.824(4)	90
β (º)	88.463(4)	90
γ (º)	88.991(4)	120
V /Å^3	1589.46(15)	4665.2(3)
D_c (g cm^{-3})	1.669	1.432
Z	2	6
μ (mm^{-1})	0.727	0.559
F (000)	808	2028
θ range (deg)	2.976- 24.997	3.120-24.994
Data/restraints/params	5593/0/442	5487/482/433
GOF on F^2	1.166	1.108
R_1^a [$I > 2\sigma(I)$], wR_2^b (all data)	0.0903, 0.2689	0.0982, 0.2582
Largest diff. peak/ hole/ e Å^{-3}	2.761/ -1.985	1.676/ -1.035

Table S2 Selected bond distances (Å) and bond angles (º) for [Ru(bpy)(Hdpa)$_2$](ClO$_4$)$_2$, [**2**](ClO)$_4$)$_2$

	[**2**](ClO$_4$)$_2$
Ru(1)-N(2)	2.079(8)
Ru(1)-N(5)	2.085(8)
Ru(1)-N(3)	2.094(8)
Ru(1)-N(1)	2.095(8)
Ru(1)-N(8)	2.097(8)
Ru(1)-N(6)	2.100(8)
N(4)-H(4)	0.86
N(7)-H(7)	0.86
N(2)-Ru(1)-N(5)	95.9(3)
N(2)-Ru(1)-N(3)	85.8(3)
N(5)-Ru(1)-N(3)	87.9(3)
N(2)-Ru(1)-N(1)	79.2(3)
N(5)-Ru(1)-N(1)	173.8(3)
N(3)-Ru(1)-N(1)	88.0(3)
N(2)-Ru(1)-N(8)	92.6(3)
N(5)-Ru(1)-N(8)	94.2(3)
N(3)-Ru(1)-N(8)	177.5(3)
N(1)-Ru(1)-N(8)	89.8(3)
N(2)-Ru(1)-N(6)	175.7(3)
N(5)-Ru(1)-N(6)	88.2(3)
N(3)-Ru(1)-N(6)	93.1(3)
N(1)-Ru(1)-N(6)	96.6(3)
N(8)-Ru(1)-N(6)	88.3(3)

Table S3 Selected bond distances (Å) and bond angles (º) for [Ru(bpy)$_2$(dpa)](BF_4), [**1**](BF_4)

	[**1**](BF_4)
Ru(1)-N(2)	2.043(11)
Ru(1)-N(3)	2.054(12)
Ru(1)-N(4)	2.066(11)
Ru(1)-N(1)	2.070(11)
Ru(1)-N(6)	2.076(12)
Ru(1)-N(5)	2.113(13)
N(2)-Ru(1)-N(3)	87.6(5)
N(2)-Ru(1)-N(4)	95.0(5)
N(3)-Ru(1)-N(4)	78.2(5)
N(2)-Ru(1)-N(1)	79.2(5)
N(3)-Ru(1)-N(1)	96.5(5)
N(4)-Ru(1)-N(1)	172.3(5)
N(2)-Ru(1)-N(6)	93.3(4)
N(3)-Ru(1)-N(6)	173.8(5)
N(4)-Ru(1)-N(6)	95.6(5)
N(1)-Ru(1)-N(6)	89.8(5)
N(2)-Ru(1)-N(5)	175.5(6)
N(3)-Ru(1)-N(5)	91.8(6)
N(4)-Ru(1)-N(5)	89.3(5)
N(1)-Ru(1)-N(5)	96.5(6)
N(6)-Ru(1)-N(5)	87.8(6)

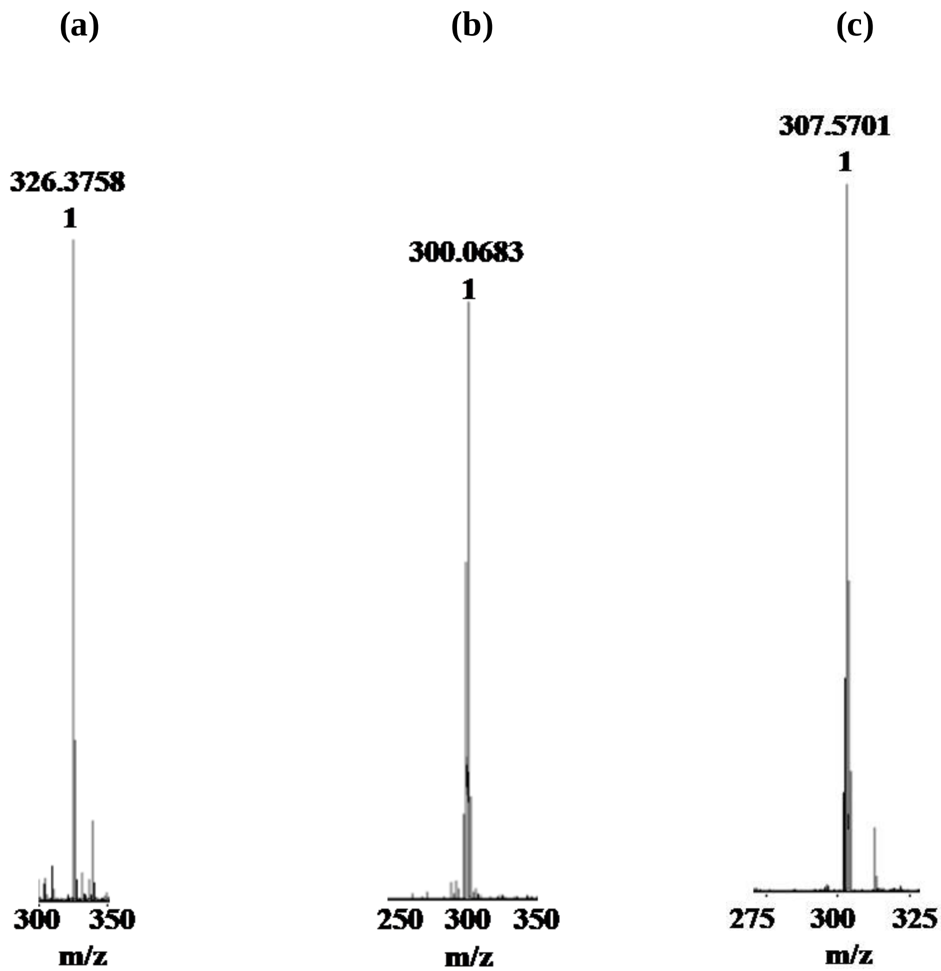

Fig. S1 ESI-MS (positive) for [**1**]$(ClO_4)_2$ (a), [**2**]$(ClO_4)_2$ (b) and [**3**]$(ClO_4)_2$ (c).

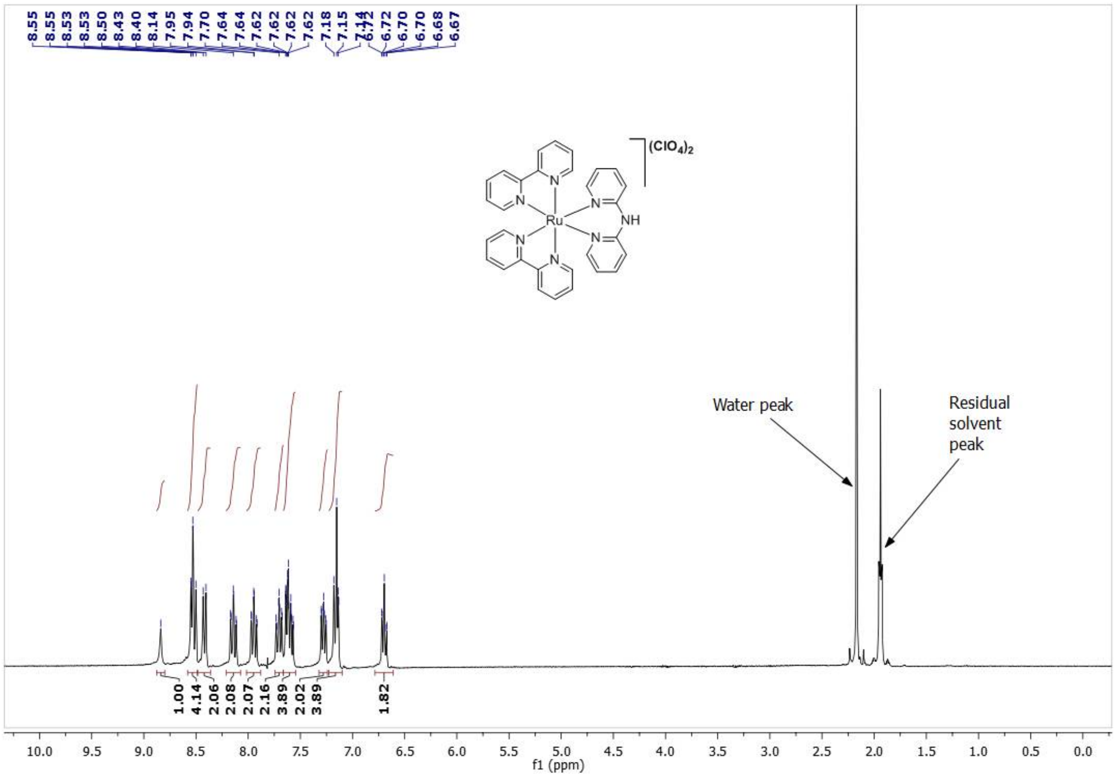

Fig. S2 ^{1}H NMR of receptor [**1**]$(ClO_4)_2$ in CD_3CN.

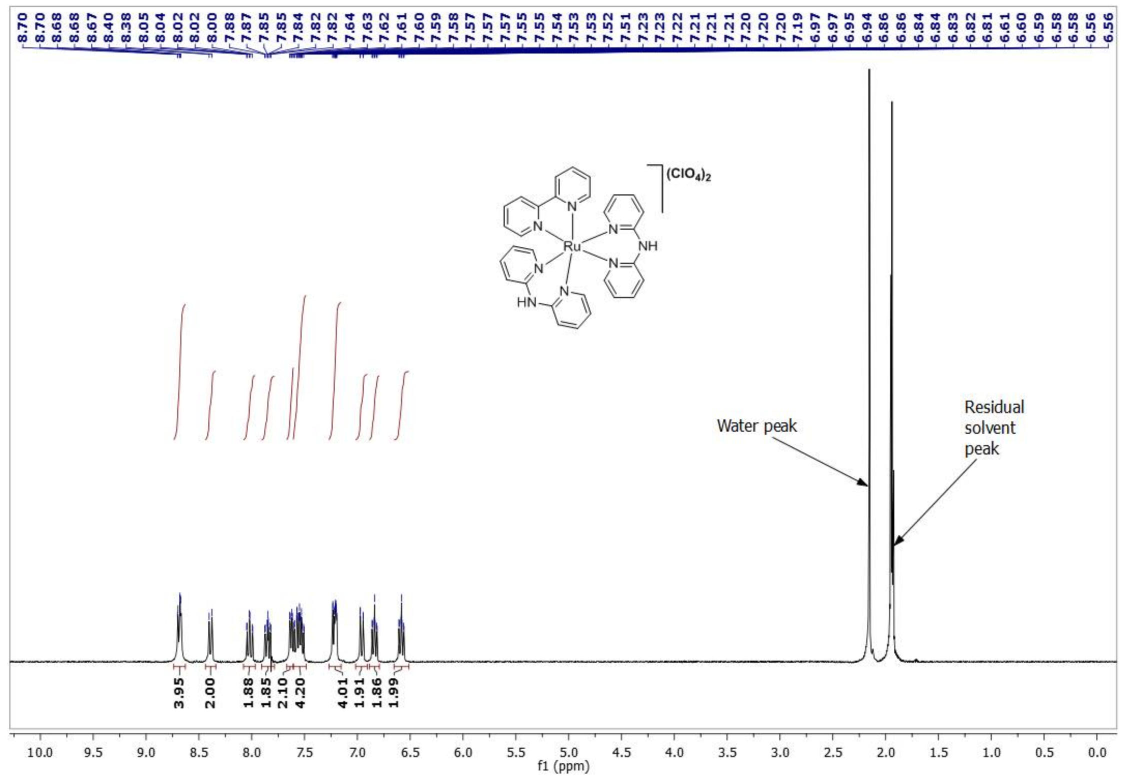

Fig. S3 ^{1}H NMR of receptor [**2**](ClO_4)$_2$ in CD_3CN.

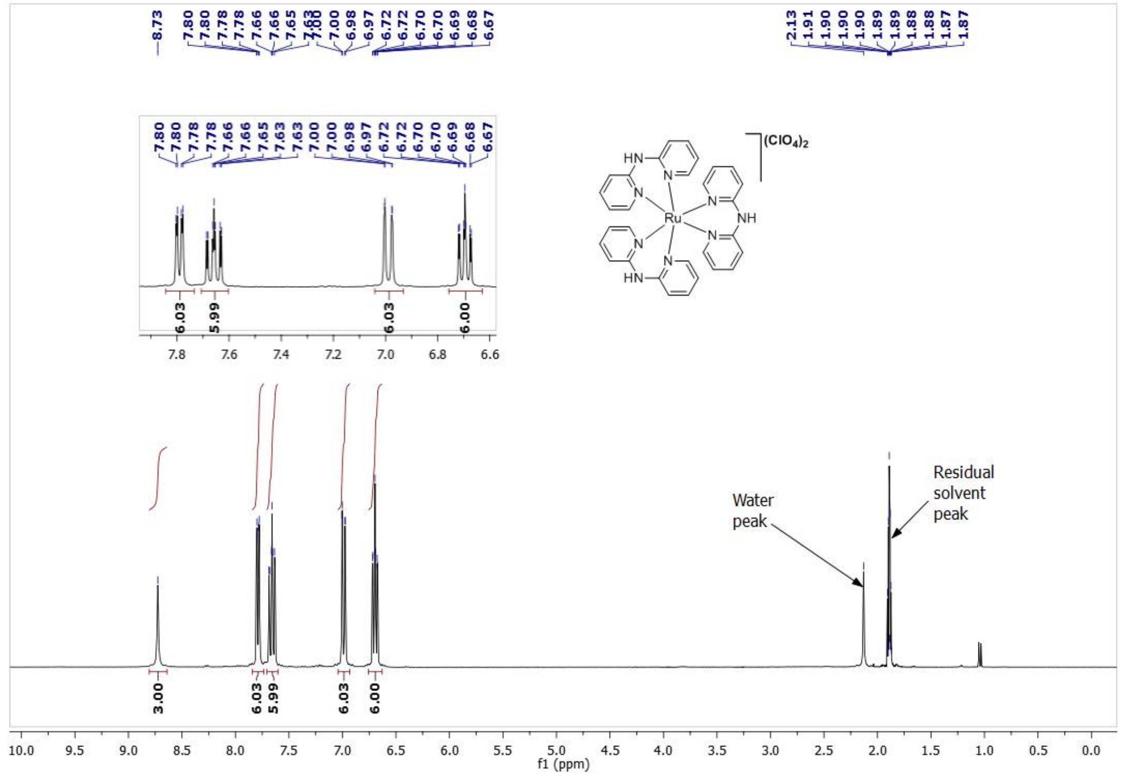

Fig. S4 ^{1}H NMR of receptor [**3**](ClO_4)$_2$ in CD_3CN.

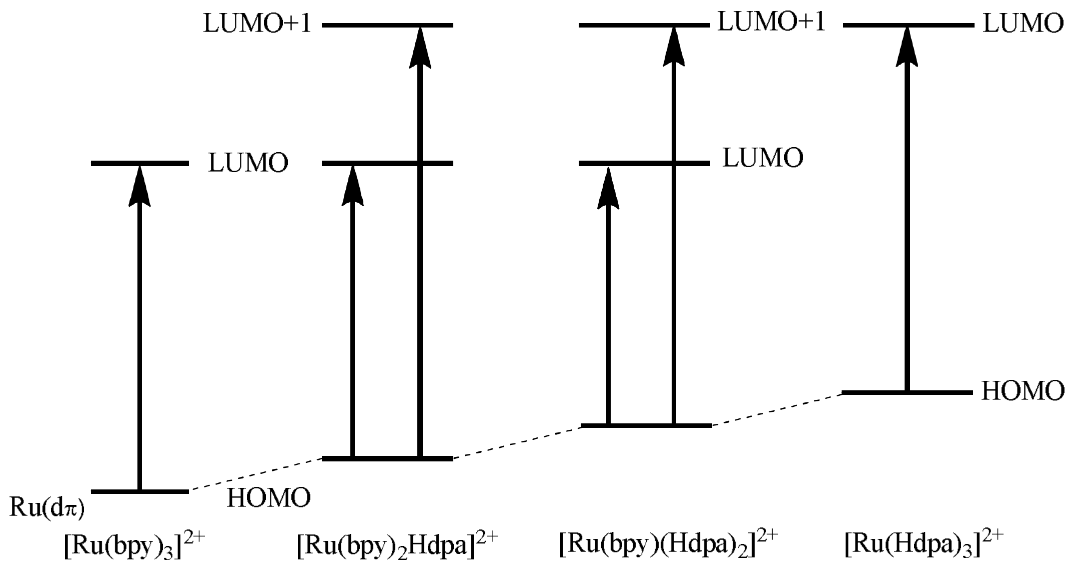

Fig. S5 Qualitative schematic energy diagram for $[Ru(bpy)_{3-n}(Hdpa)_n](ClO_4)_2$, where n = 0-3.

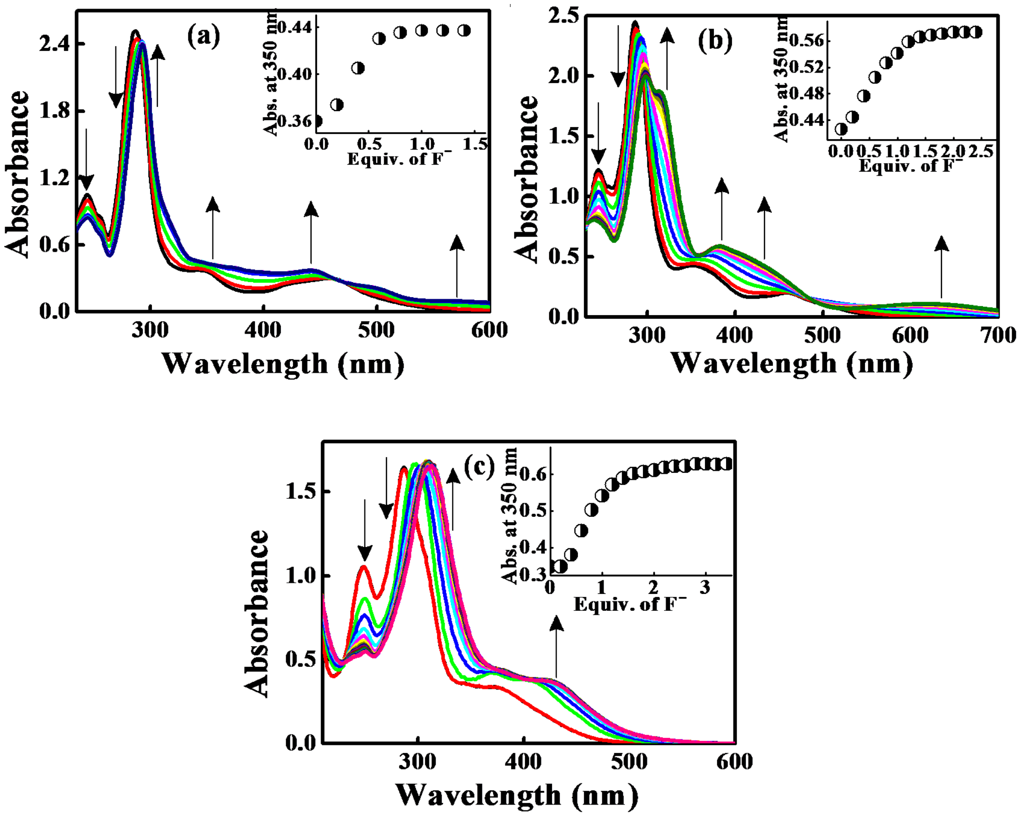

Fig. S6 Changes in absorption spectra of receptor $\mathbf{1}^{2+}$ (a), $\mathbf{2}^{2+}$ (b) and $\mathbf{3}^{2+}$ (c) in CH_3CN upon addition of F^{-}. The inset shows the changes of absorbance as a function of the equivalents of F^{-} added.

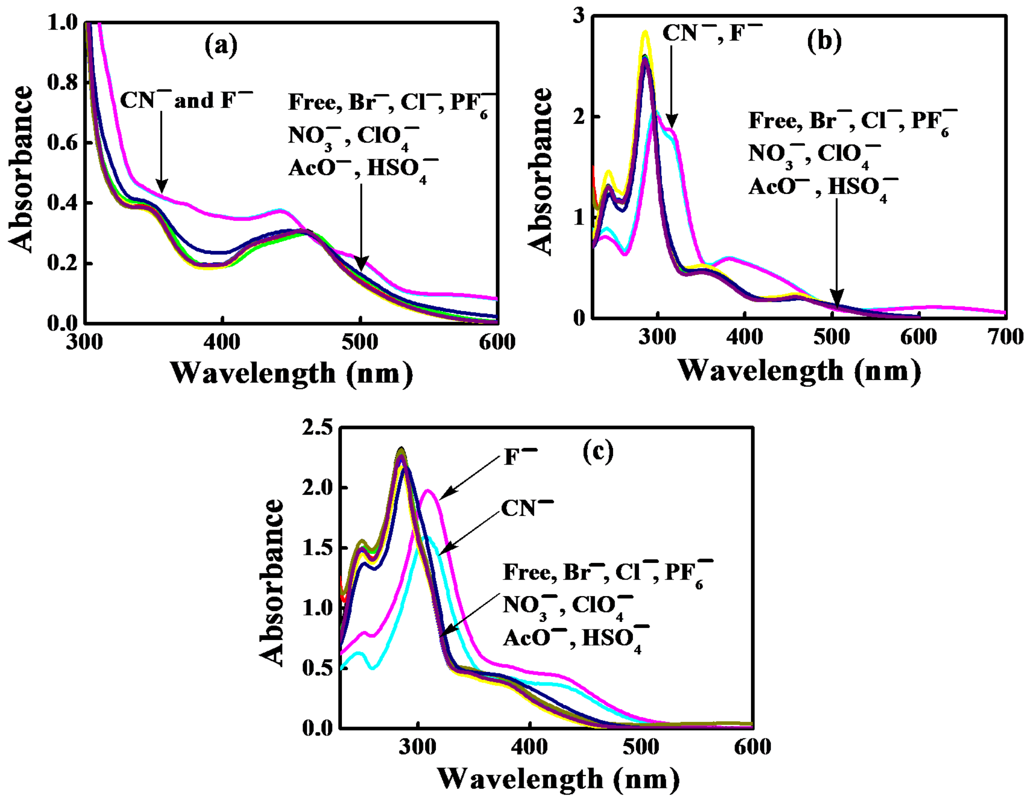

Fig. S7 Changes in absorption spectra of receptor $\mathbf{1}^{2+}$ (a), $\mathbf{2}^{2+}$ (b) and $\mathbf{3}^{2+}$ (c) in CH_3CN in addition of different anions as their TBA–salts.

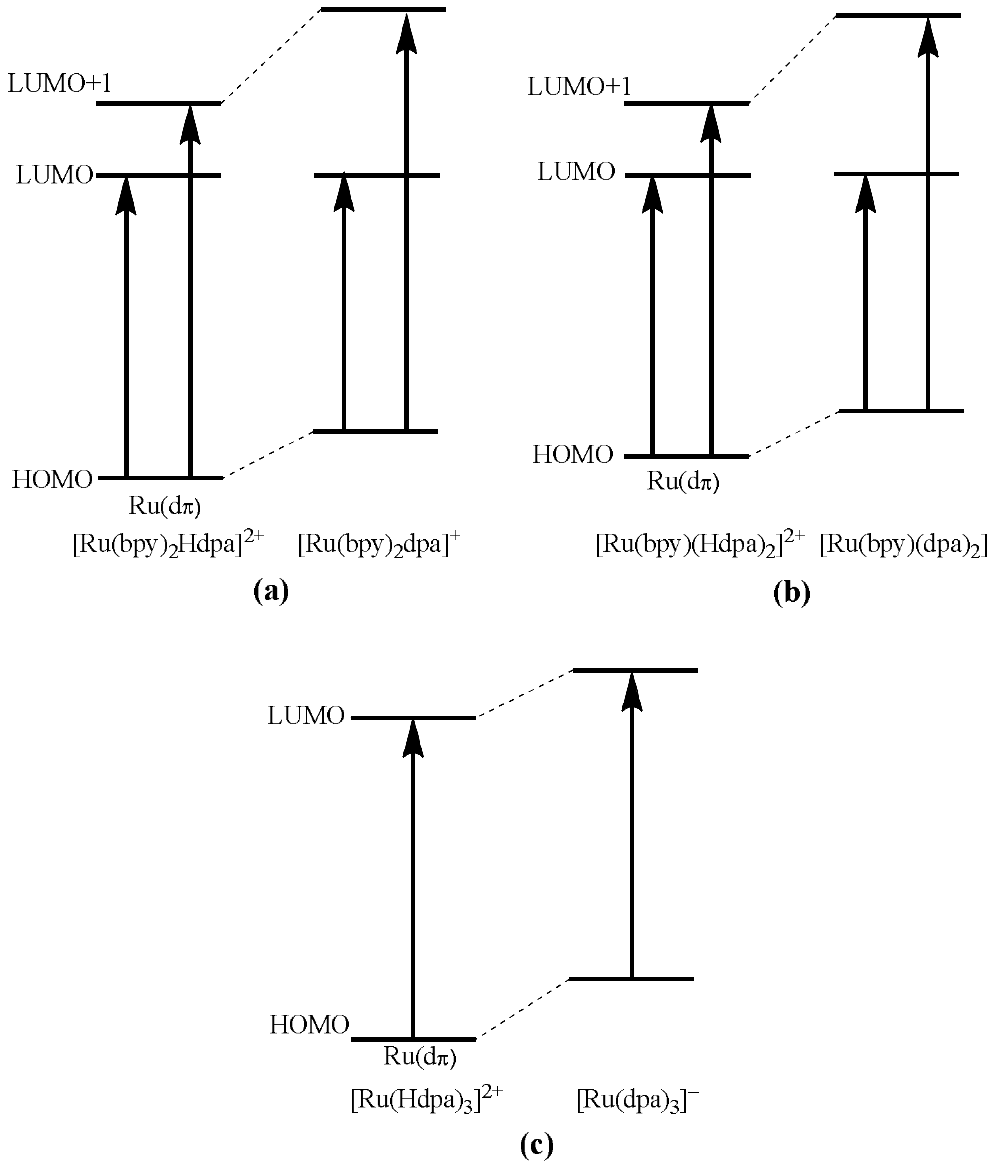

Fig. S8 Qualitative energy diagram for $[Ru(bpy)_{3-n}(Hdpa)_n](ClO_4)_2$, where n = 1-3, with corresponding deprotonated complexes.

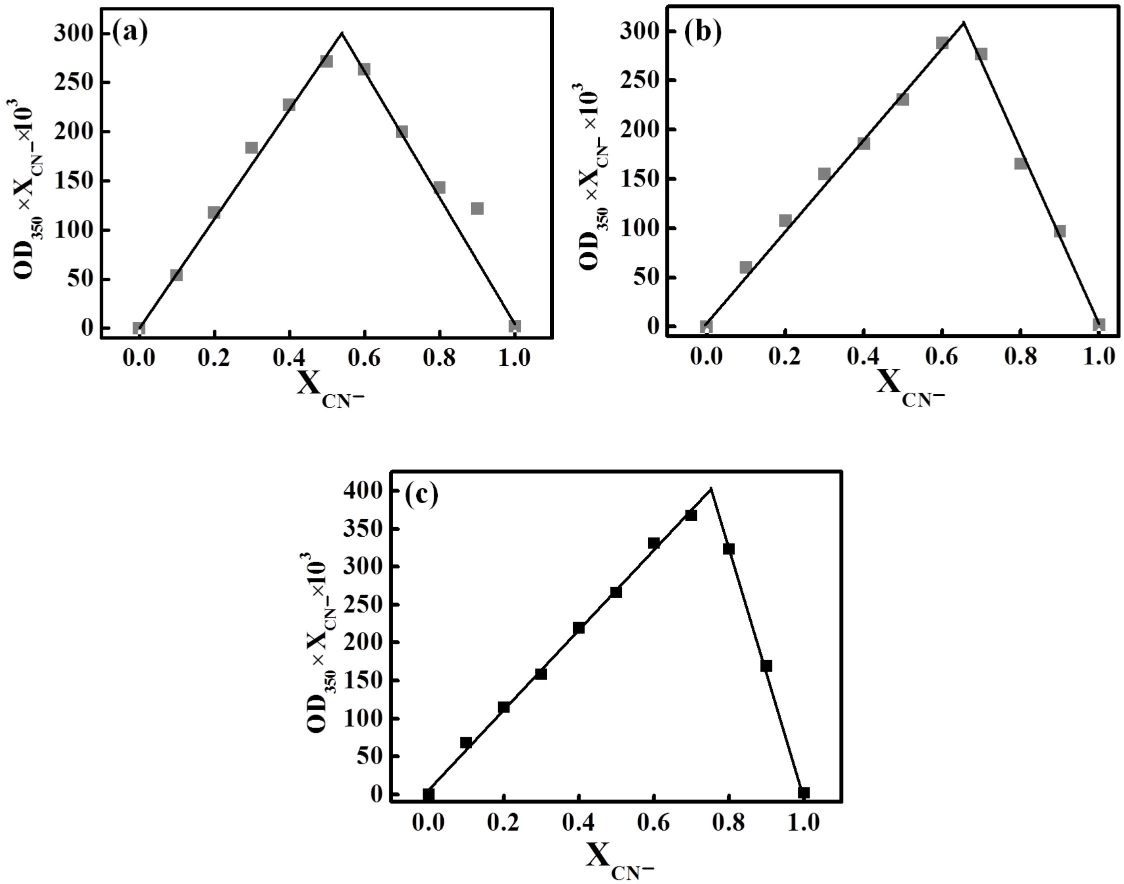

Fig. S9 Job plots for the determination of the stoichiometry of **1**$^{2+}$ (a), **2**$^{2+}$ (b) and **3**$^{2+}$ (c) with CN^- ion.

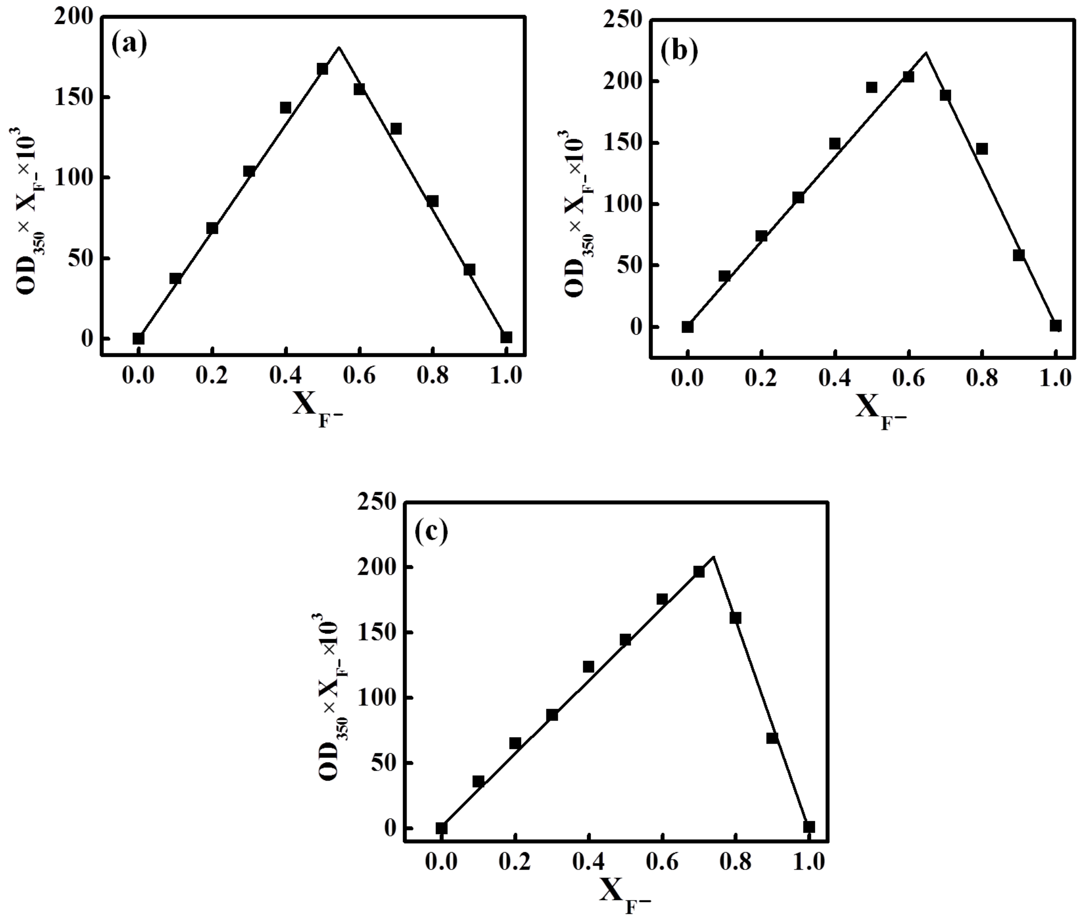

Fig. S10 Job plots for the determination of the stoichiometry of $\mathbf{1}^{2+}$ (a), $\mathbf{2}^{2+}$ (b) and $\mathbf{3}^{2+}$ (c) with F^{-} ion.

.

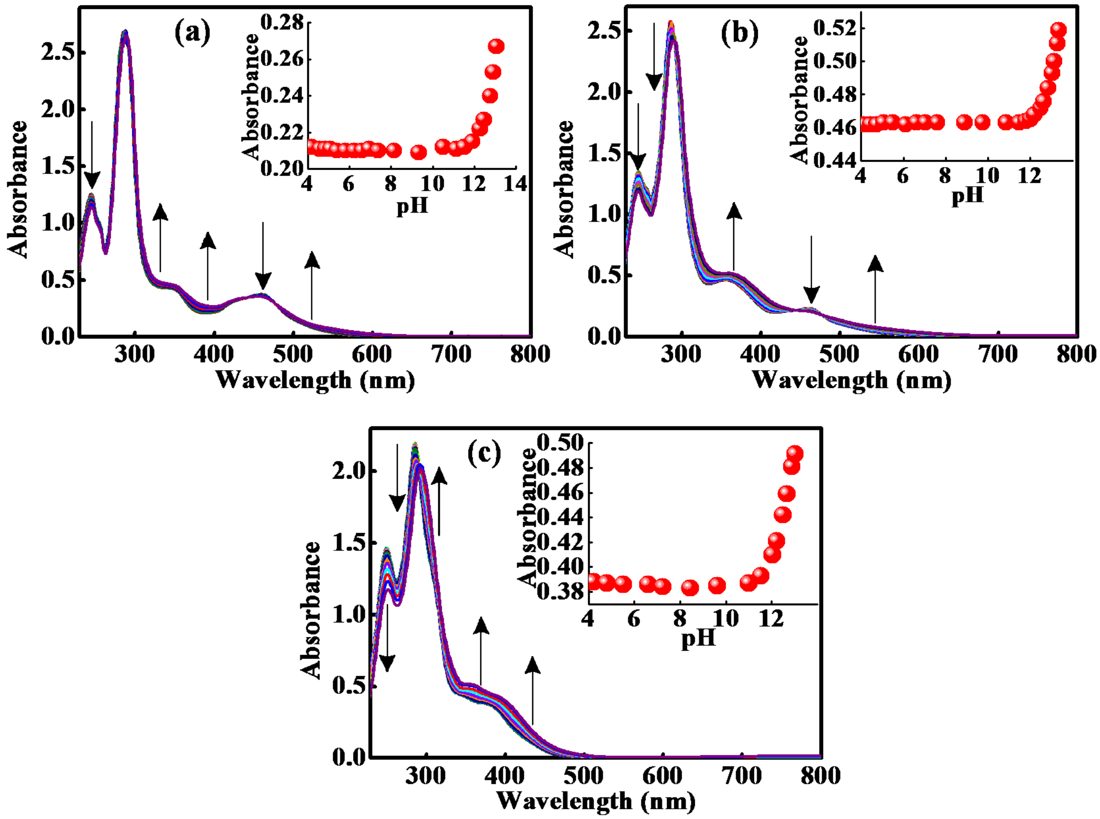

Fig. S11 Absorption spectra of (a) $\mathbf{1}^{2+}$ (b) $\mathbf{2}^{2+}$ and (c) $\mathbf{3}^{2+}$ as a function of pH in Britton-Robinson aqueous universal buffer solution. Insets show the changes in absorbance at (a) 398 nm for $\mathbf{1}^{2+}$, (b) 360 nm for $\mathbf{2}^{2+}$ (c) 368 nm for $\mathbf{3}^{2+}$ with the pH.

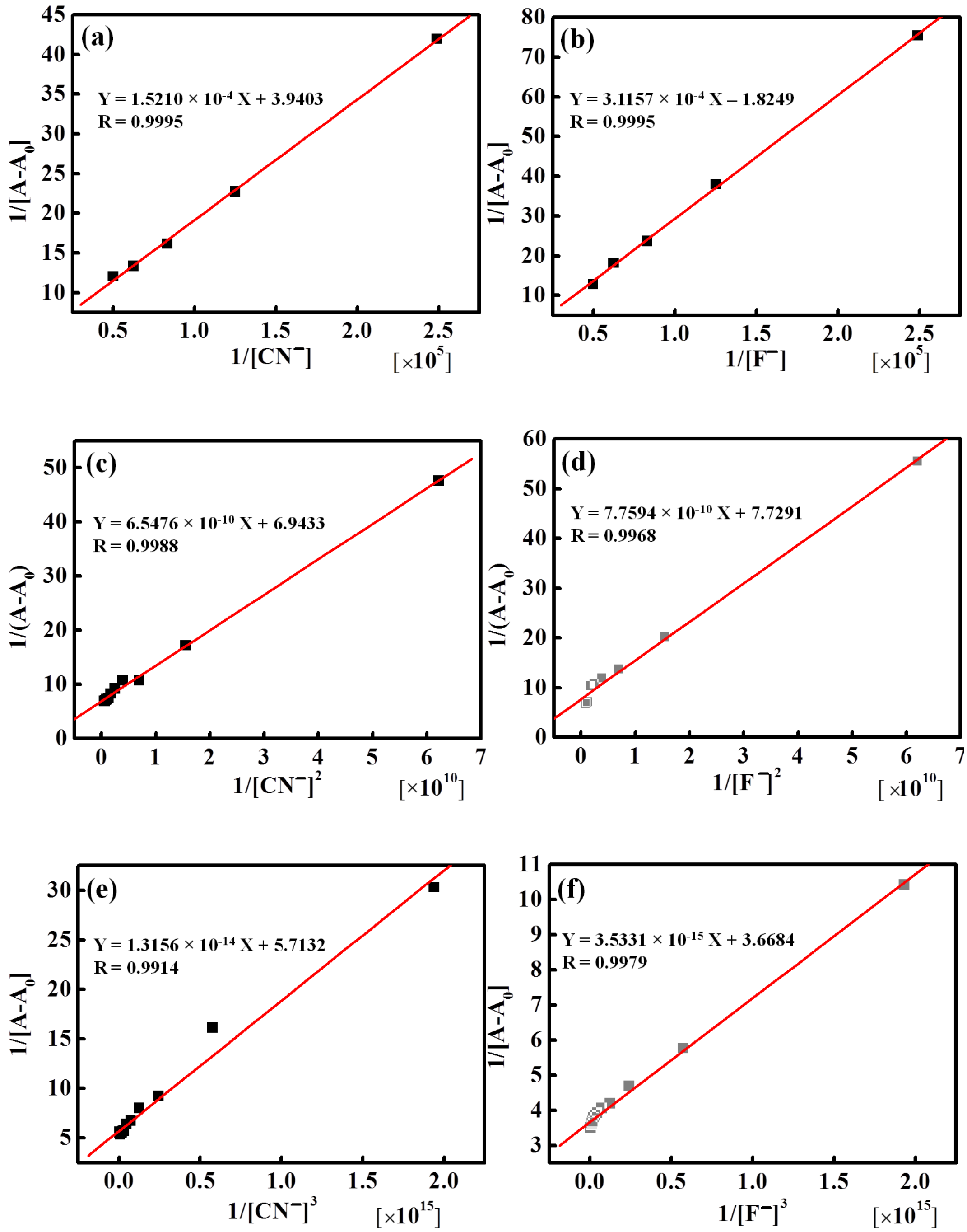

Fig. S12 Benesi-Hildebrand plots (a-f) of $\mathbf{1}^{2+}$, $\mathbf{2}^{2+}$ and $\mathbf{3}^{2+}$ with CN^{-} and F^{-} .

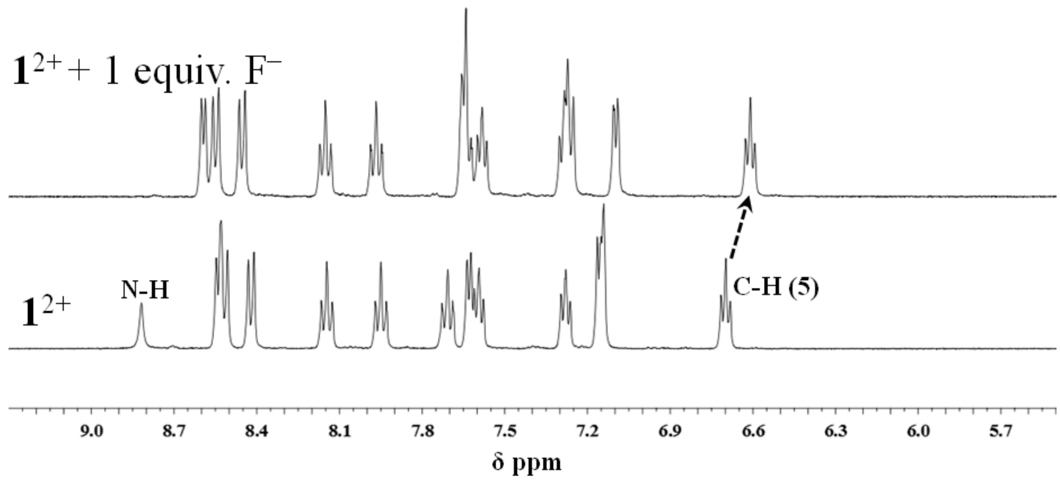

Fig. S13 ^{1}H NMR spectra of $\mathbf{1}^{2+}$ in absence and presence of one equivalent of F^- in CD_3CN.

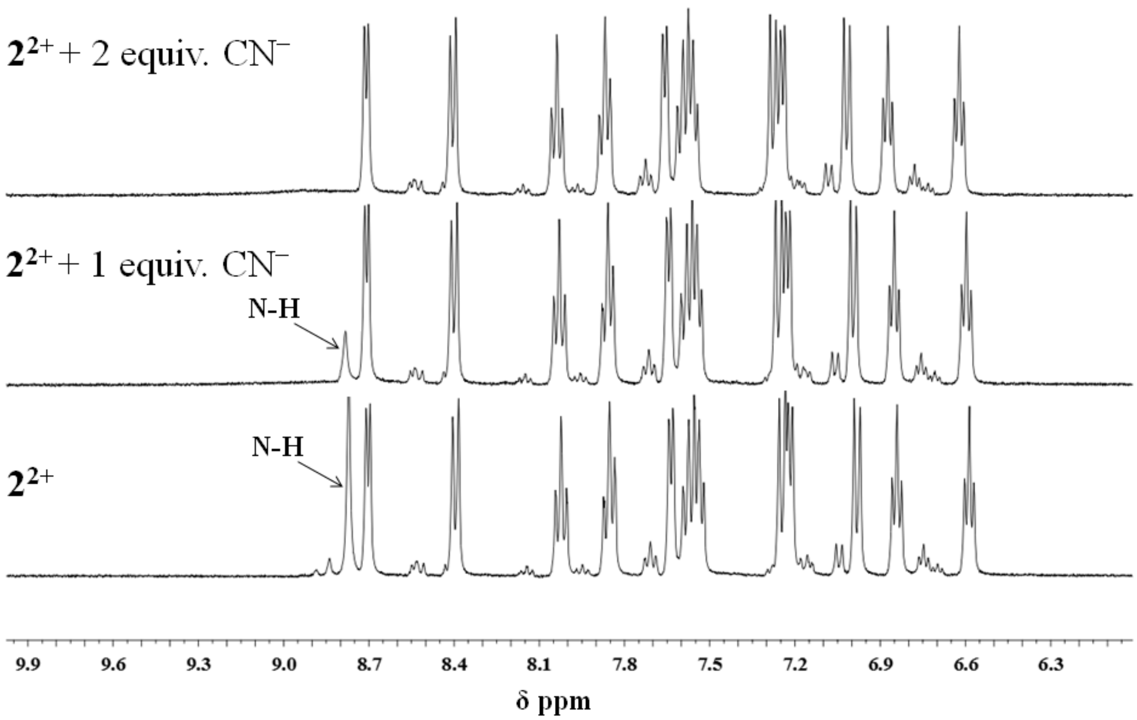

Fig. S14 ^{1}H NMR titration of $\mathbf{2}^{2+}$ in CD_3CN with the TBA salt of CN^- ion (0–2 equivalents).

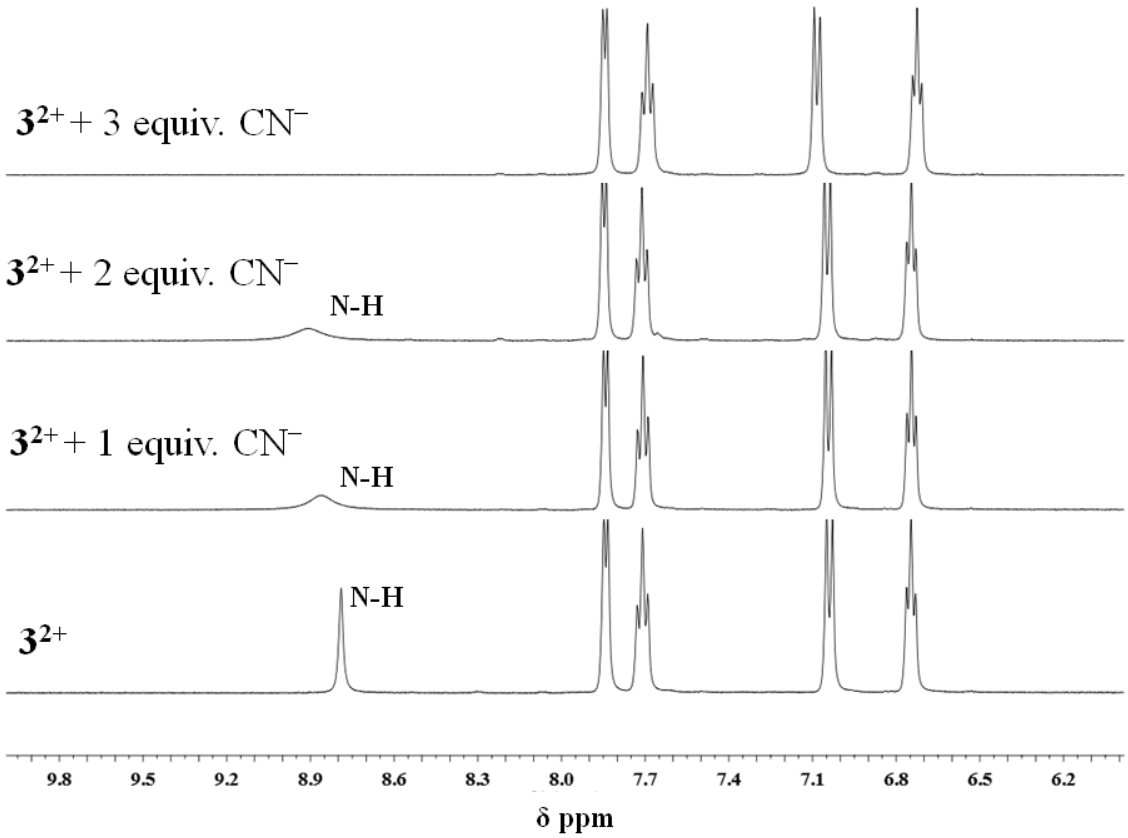

Fig. S15 ^{1}H NMR titration of **3**$^{2+}$ in CD_3CN with the TBA salt of CN^- ion (0–3 equivalents).

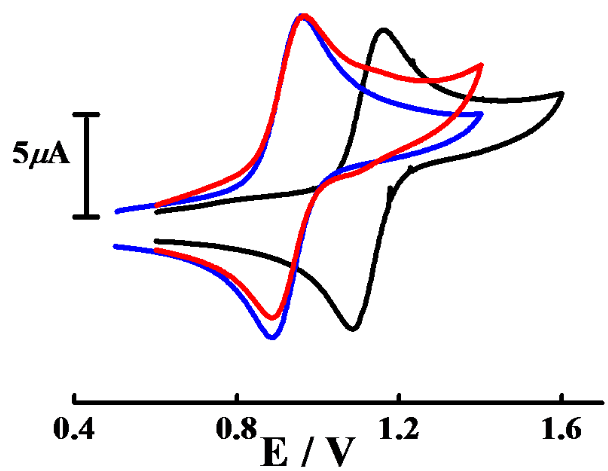

Fig. S16 Cyclic voltammograms of $\mathbf{1}^{2+}$ (black), $\mathbf{2}^{2+}$ (red) and $\mathbf{3}^{2+}$ (blue) in CH_3CN.

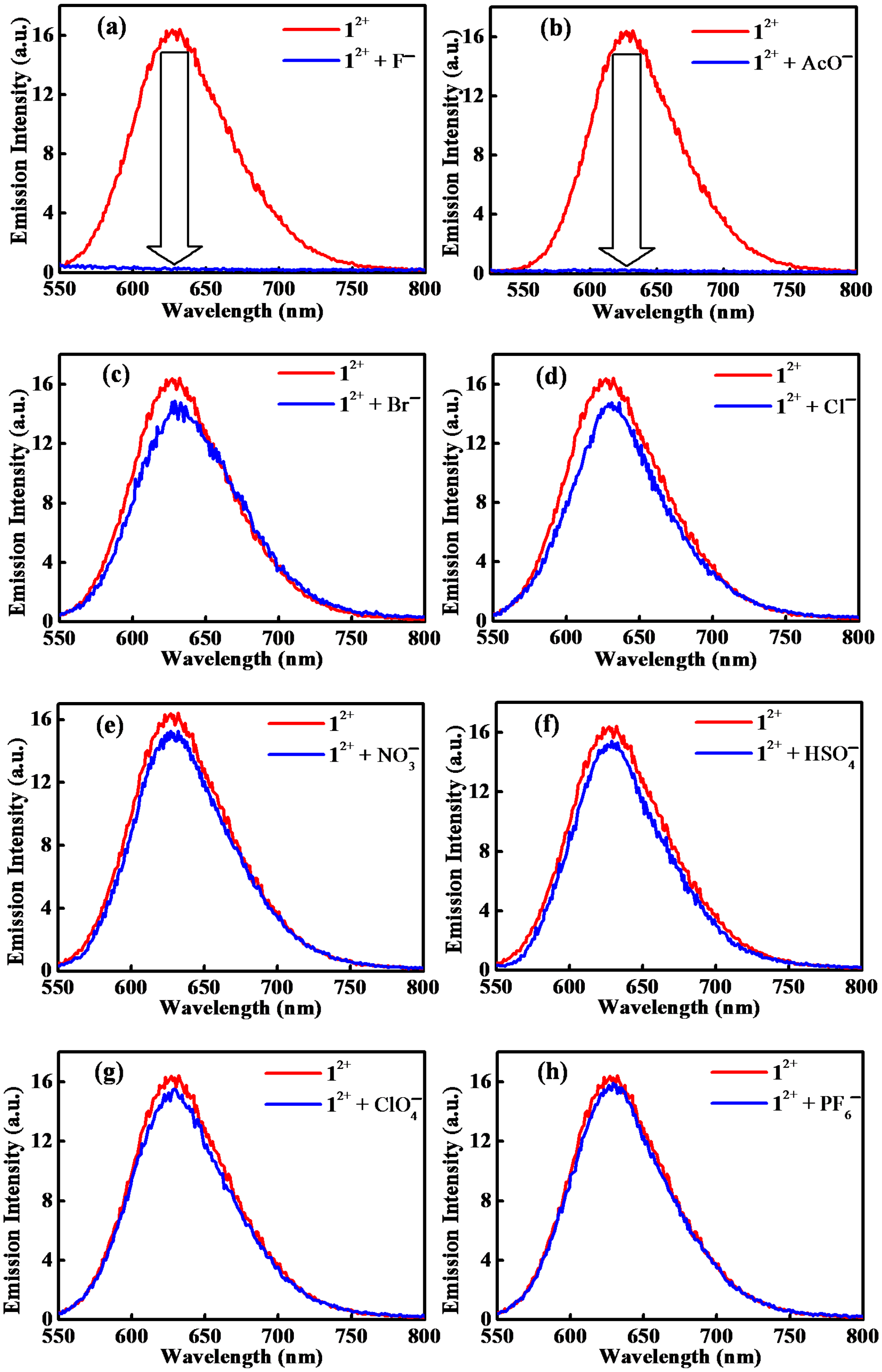

Fig. S17 Changes in emission intensity of receptor $\mathbf{1}^{2+}$ upon addition of TBA–salts of different anions.

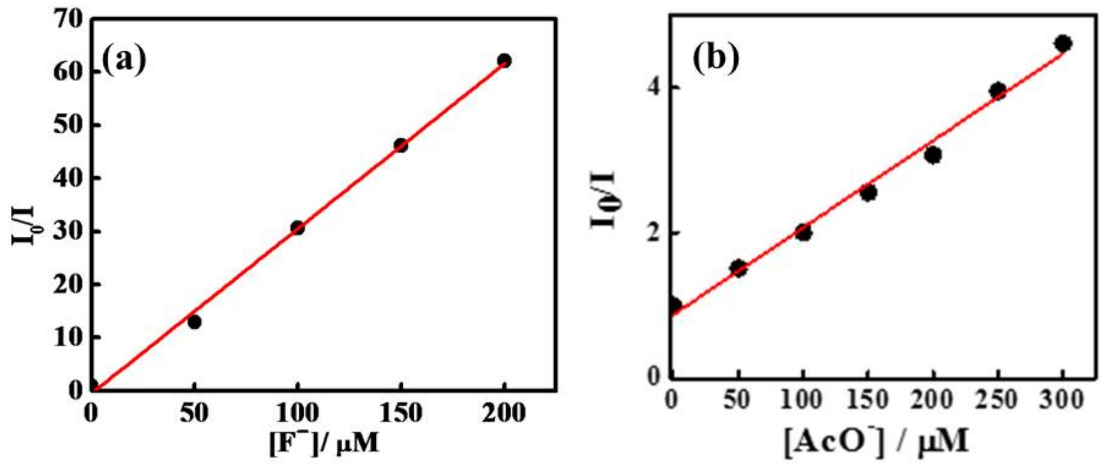

Fig. S18 Stern-Volmer plots of [**1**]$(ClO_4)_2$ with F^-(a) and AcO^- (b).

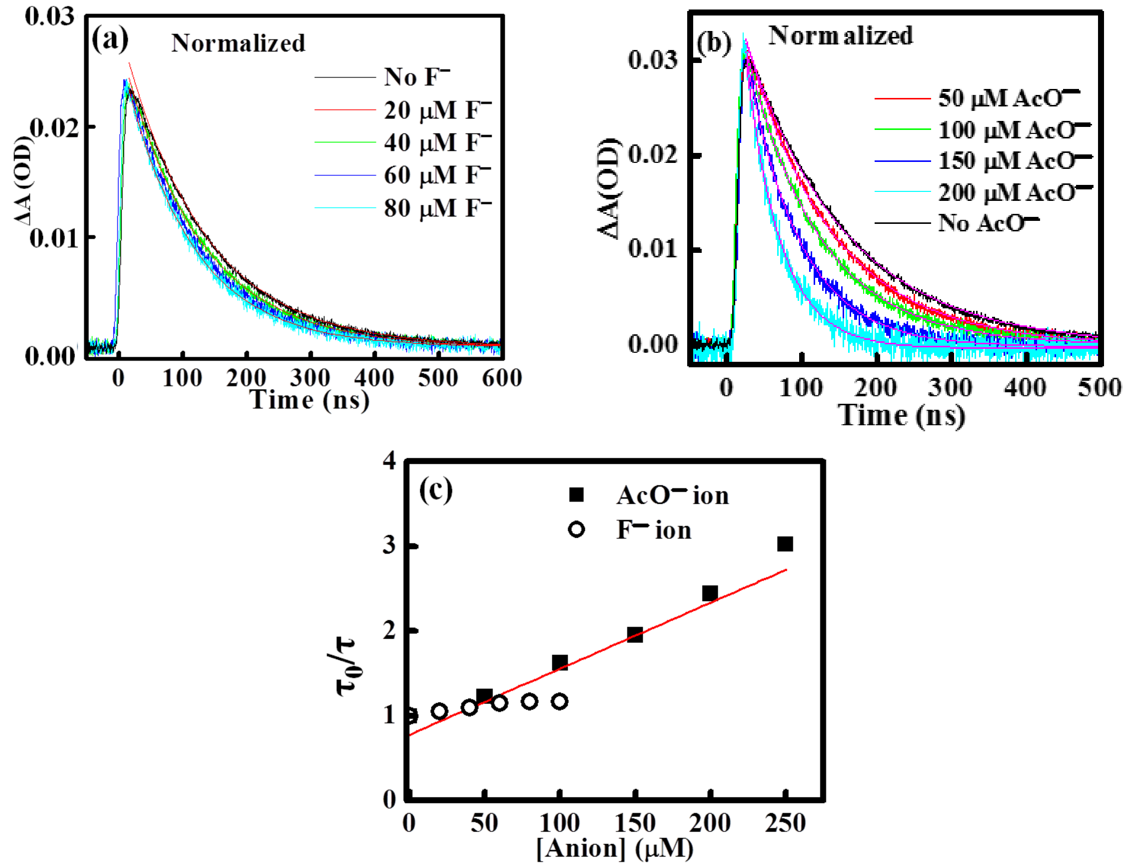

Fig. S19 Emission kinetics (normalized at maxima) of complex [**1**](ClO_4)$_2$ in presence of F^- (a) and AcO^- (b) ion. (c) Plot of τ_0/τ versus concentration of anions (F^- and AcO^-).

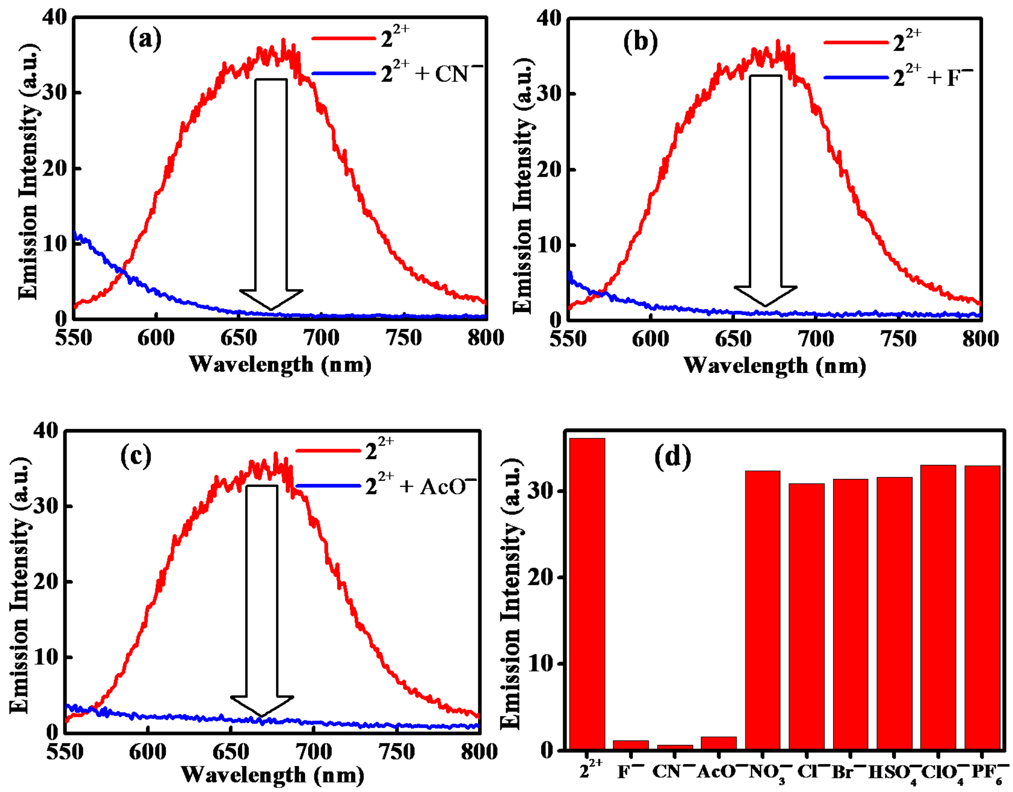

Fig. S20 Emission spectra of receptor $\mathbf{2}^{2+}$ in CH_3CN solution in the presence and absence of CN^- (a), F^- (b) and AcO^- (c) anions. (d) Relative emission intensity of receptor $\mathbf{2}^{2+}$ upon addition of F^-, CN^-, AcO^-, NO_3^-, Cl^-, Br^-, HSO_4^-, ClO_4^- and PF_6^- ions in CH_3CN solution.

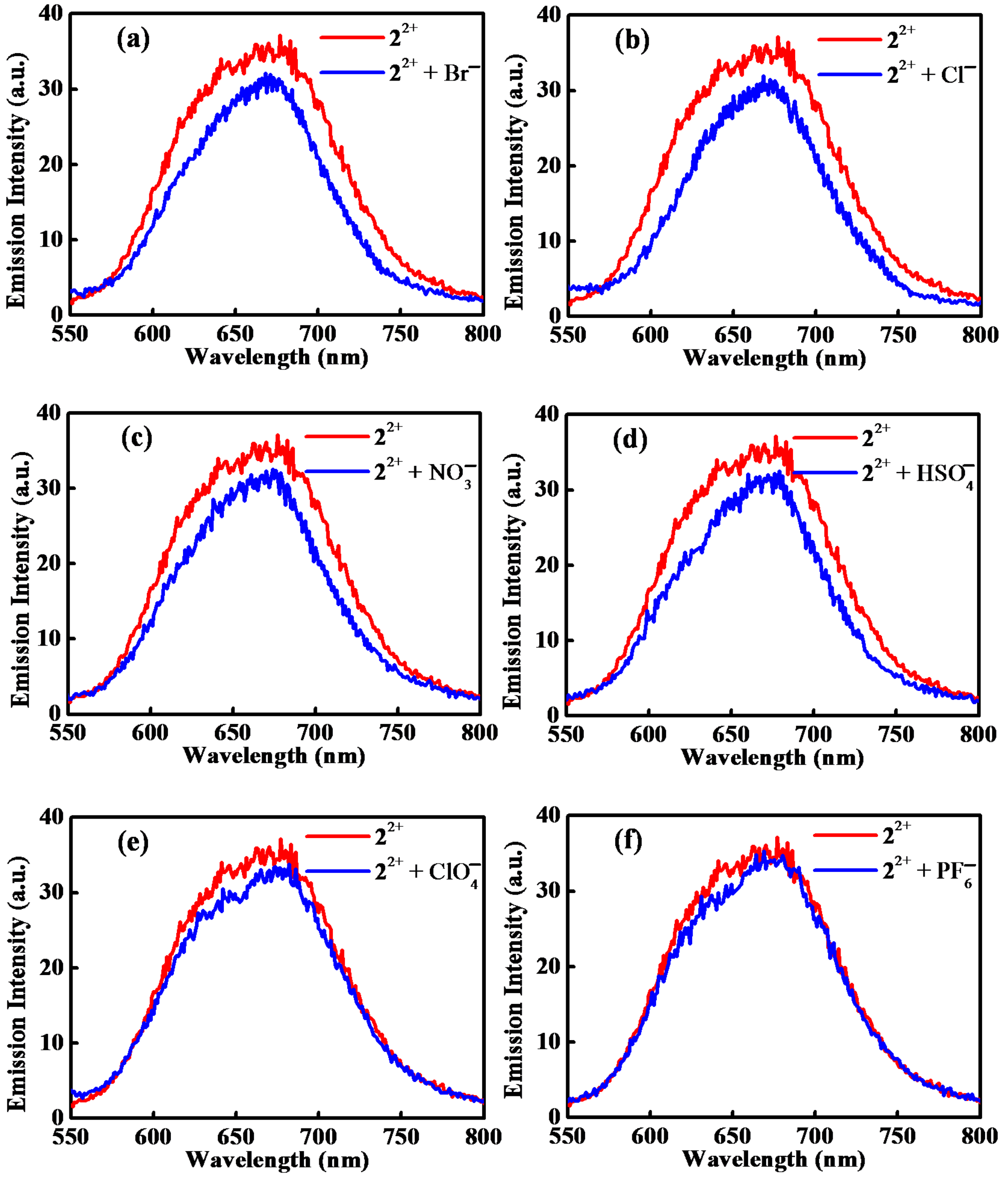

Fig. S21 Changes in emission spectra of receptor $\mathbf{2}^{2+}$ upon addition of different anions of TBA–salts.